Journal of
Composites Science

MDPI

Article

Impact of Moisture Absorption on Optical Fiber Sensors: New Bragg Law Formulation for Monitoring Composite Structures

Pietro Aceti * and Giuseppe Sala

Department of Aerospace Science and Technology, Politecnico di Milano, Via La Masa n. 34, 20156 Milan, Italy; giuseppe.sala@polimi.it
* Correspondence: pietro.aceti@polimi.it

Abstract: In recent decades, the aviation industry has increasingly adopted composite materials for various aircraft components, due to their high strength-to-weight ratio and durability. To ensure the safety and reliability of these structures, Health and Usage Monitoring Systems (HUMSs) based on fiber optics (FO), particularly Fiber Bragg Grating (FBG) sensors, have been developed. However, both composite materials and optical fibers are susceptible to environmental factors such as moisture, in addition to the well-known effects of mechanical stress and thermal loads. Moisture absorption can lead to the degradation of mechanical properties, posing a risk to the structural integrity of aircraft components. This research aims to quantify and monitor the impact of moisture on composite materials. A new formulation of the Bragg equation is introduced, incorporating mechanical strain, thermal expansion, and hygroscopic swelling to accurately measure Bragg wavelength variations. Experimental validation was performed using both uncoated and polyimide-coated optical fibers subjected to controlled hygrothermal conditions in a climate chamber. The results demonstrate that uncoated fibers are insensitive to humidity, whereas coated fibers exhibit measurable wavelength shifts due to moisture absorption. The proposed model effectively predicts these shifts, with errors consistently below 2.6%. This approach is crucial for improving the performance and reliability of HUMSs in monitoring composite structures, ensuring long-term safety in extreme environmental conditions.

Keywords: optical fiber; FBG sensors; hygrothermal effects; Bragg equations; Health and Usage Monitoring System

Citation: Aceti, P.; Sala, G. Impact of Moisture Absorption on Optical Fiber Sensors: New Bragg Law Formulation for Monitoring Composite Structures. *J. Compos. Sci.* **2024**, *8*, 518. https://doi.org/10.3390/jcs8120518

Academic Editor: Sambandam Anandan

Received: 28 October 2024
Revised: 27 November 2024
Accepted: 5 December 2024
Published: 9 December 2024

1. Introduction

One of the most significant steps forward in aeronautical science has been taken in recent decades thanks to the use of composite materials. These are characterized by higher mechanical properties (strength, stiffness, and fatigue resistance above all) compared to traditional aluminum alloys, but also by other advantages such as a higher strength-to-weight ratio, corrosion and impact resistance, design and production process flexibility, low thermal expansion coefficient, and high temperature resistance [1–4]. Composite materials are widely used in the aerospace sector for primary structures such as fuselage, empennages, governing surfaces, wing but also for other non-structural interior aircraft parts [5–7]. The main reason of the adoption of composites in the aerospace field is their light weight compared to traditional configurations, considering that weight is the main parameter taken into account during the design process of an aircraft, since it contributes to the consumption of less fuel, leading to economic savings for airline companies. Moreover, it must be considered that the attention to reducing emissions is also one of the main concerns for the actual aircraft market, with increasing interest among airlines in sustainability and green fuel trends. However, the use of composite structures is not without drawbacks: in fact, they are in direct contact with the external environment, so they easily interact with atmospheric agents or water and are more prone to moisture damage during their operations. Moisture uptake leads to detrimental effects on mechanical, physical, electrical,thermal properties

and service life reduction [8,9]. In [10], it has been observed that some advanced composite structural components, like sandwich panels and adhesive bonded joints, have a conformation, from the morphological and design point of view, that tends to enhance the moisture ingress, since they are not perfectly isolated from the external environment and are realized by connecting several parts together (laminate layers, substrates, adhesives,honeycomb core), with higher risk of water penetration at the interfaces and consequently delamination due to freeze–thaw cycles [11]. Some examples of in-flight failures due to hygrothermal issues can be found in the literature: Figure 1a shows the state of Concorde after the loss of the rudder in flight on 14 April 1989 [3,12]. Subsequent investigations showed that the main cause of the accident was the absorption of moisture, which exacerbated the effects of the defect presented in the component since the manufacturing phase. Figure 1b shows the A310 Polaris after suffering in-flight damage that resulted in the loss of an elevator on 8 May 2015. Moreover, post-accident investigations revealed that moisture uptake and high temperatures were the main cause of the accident [13,14]. Moisture absorbed within the composite elements acts as a plasticizer, degrading the mechanical properties of the composite and severely impacting the performance of the aircraft. Since reliability standards must be kept high to satisfy the requirements imposed by aviation regulations, effective solutions to the problem of humidity and hygrothermal aging must be adopted to guarantee safe operations and extend the operational life of composite structural components.

(**a**) Concorde accident on 14 April 1989 (**b**) A310 Polaris accident on 8 May 2015

Figure 1. Accidents due to hygrothermal effects.

Optical fiber-based HUMS/SHM systems are among the most widely employed in the inherent advantages of the aerospace sector, such as low cost, small size, real-time response, high accuracy, high sensitivity, and immunity to electromagnetic interference. They are able to sense various quantities, such as temperature, pressure, and strain, using grating-based devices (BGDs) [15,16]. Optical fibers are frequently embedded within composite materials, which, as previously discussed, are prone to moisture absorption. Consequently, optical fibers and their coatings are also susceptible to moisture uptake. The issue of moisture absorption by polyimide coatings has been reported in the literature, for example, in [17,18].

One of the objectives of the present work is to verify that the polyimide used to coat optical fibers for sensing—therefore requiring excellent load transfer capabilities—experiences the same effects. The swelling of the fiber coating resulting from moisture absorption can influence the signal reflected by the optical fiber, thus affecting the accuracy of the measurements. To ensure precise measurements, it is essential to account for the swelling induced by moisture absorption. The primary objective of this paper is to propose a modified Bragg's law that incorporates the effects of mechanical deformation, thermal expansion, and moisture-induced swelling. In the literature, there are formulations that attempt to account for the strains introduced by humidity in the optical fiber [18,19]. These formulations differ from the one proposed in this paper, as they consider thermal expansion as if it were a strain caused by an external force acting on the fiber; therefore, they multiply it by the photo-elastic coefficient. However, as will be presented below, the photo-elastic coefficient should only be multiplied by the strain generated by a real stress fields, as it represents the relationship between the refractive index and stress, and not by

that generated by thermal expansion, which, by definition, occurs under zero stress. Therefore, in the present formulation, unlike others, the photo-elastic coefficient will only multiply the deformation generated by actual stress or residual stress.

2. Theoretical Formulation

In this chapter, a new formulation of the Bragg's law (Equation (1)) is presented for an uncoated optical fiber in Section 2.1 and for a coated optical fiber in Section 2.2. The method consists of differentiating the Bragg equation, analyzing the effects of each measurable quantity on the signal wavelength, and translating these effects to the sensing element using the rules of mixtures and the compatibility equation. This approach allows for an accurate assessment of the Bragg wavelength variation, effectively mitigating potential measurement errors caused by moisture absorption.

2.1. Uncoated Optical Fiber

Fiber Bragg Gratings were first studied by Kenneth O.Hill in 1978 [20] at the Communication Research Centre of Canada. Bragg's law, initially developed for the propagation of light in crystals, has been rearranged in the form presented in Equation (1) to explain the behavior of FBG sensors inscribed in an uncoated optical fiber:

$$\lambda = 2n_{eff}\Lambda \tag{1}$$

where λ is the wavelength reflected by a FBG sensor inscribed in an uncoated optical fiber characterized by an effective refractive index equal to n_{eff} and a distance between two gratings (i.e., pitch distance) equal to Λ.

Considering now a quantity X that needs to be measured, its effect on the n_{eff} and Λ of the FBG can be evaluated by deriving the Bragg law (Equation (1)):

$$\frac{\partial \lambda}{\partial X} = 2\Lambda\frac{\partial n_{eff}}{\partial X} + 2n_{eff}\frac{\partial \Lambda}{\partial X} \tag{2}$$

Knowing the wavelength reflected λ_B under any given conditions, noting that $\frac{\lambda_B}{\Lambda} = 2n_{eff}$ and $\frac{\lambda_B}{n_{eff}} = 2\Lambda$ and transforming Equation (2) into finite differences, it gives

$$\frac{\Delta\lambda}{\lambda_B} = \frac{\partial n_{eff}}{\partial X}\frac{1}{n_{eff}}\Delta X + \frac{\partial \Lambda}{\partial X}\frac{1}{\Lambda}\Delta X \tag{3}$$

where the first term links the change of the refraction index (n_{eff}) due to the variation of the quantity X to the variation of the normalized wavelength's shift ($\frac{\Delta\lambda}{\lambda_B}$). The second term links the change of the pitch (Λ) due to the variation of the quantity X to the variation of the normalized wavelength's shift ($\frac{\Delta\lambda}{\lambda_B}$). $\Delta X = X - X_B$, where ΔX represents the difference between the measured value of X at the time of measurement and the reference value X_B, at which the reference wavelength λ_B was measured. In the same way, $\Delta\lambda = \lambda - \lambda_B$.

Taking quantity X as temperature (T), we obtain

$$\frac{\Delta\lambda}{\lambda_B} = \frac{\partial n_{eff}}{\partial T}\frac{1}{n_{eff}}\Delta T + \frac{\partial \Lambda}{\partial T}\frac{1}{\Lambda}\Delta T \tag{4}$$

where $\Delta T = T - T_B$. Knowing that $\frac{\partial n_{eff}}{\partial T}\frac{1}{n_{eff}} = \xi$ is the thermo-optic coefficient that links the temperature change with the variation of refractive index and $\frac{\partial \Lambda}{\partial T}\frac{1}{\Lambda} = \alpha_g$ is the coefficient of thermal expansion of the glass, we get the photo-thermal law for an uncoated optical fiber:

$$\frac{\Delta\lambda}{\lambda_B} = \xi\Delta T + \alpha_g\Delta T \tag{5}$$

In the same way, taking quantity X as an applied displacement (l), we obtain

$$\frac{\Delta\lambda}{\lambda_B} = \frac{\partial n_{eff}}{\partial l}\frac{1}{n_{eff}}\Delta l + \frac{\partial \Lambda}{\partial l}\frac{1}{\Lambda}\Delta l \tag{6}$$

where $\Delta l = l - l_B$. Knowing that $\frac{\partial n_{eff}}{\partial l}\frac{1}{n_{eff}} l_B = -p_e$ is the photo-elastic coefficient that links the strain with the refractive index variation and $\frac{\partial \Lambda}{\partial l}\frac{1}{\Lambda}\Delta l = \varepsilon_m$ is exactly the strain applied on the optical fiber, we obtain the photo-elastic law for an uncoated optical fiber:

$$\frac{\Delta\lambda}{\lambda_B} = -p_e\varepsilon_m + \varepsilon_m \tag{7}$$

Taking quantity X as relative humidity (RH), we obtain

$$\frac{\Delta\lambda}{\lambda_B} = 0 \tag{8}$$

Rajan G. in [21] states that glass cannot absorb humidity. This implies that there is no mass uptake and consequentially no swelling occurring inside the optical fibers; this means that $\frac{\partial \Lambda}{\partial RH}\frac{1}{\Lambda} = 0$. Moreover, since there is no moisture uptake, there is no possibility to change the effective refraction index: it can be written as $\frac{\partial n_{eff}}{\partial RH}\frac{1}{n_{eff}} = 0$. This shows that, since the glass is unable to absorb humidity, an uncoated optical fiber is insensitive to relative humidity.

2.2. Coated Optical Fiber

Due to their intrinsic fragility, optical fibers are often coated with polymer coatings that are designed to protect the fiber during operational conditions or during installation when embedded in composite materials during manufacturing. A typical coated optical fiber is represented in Figure 2.

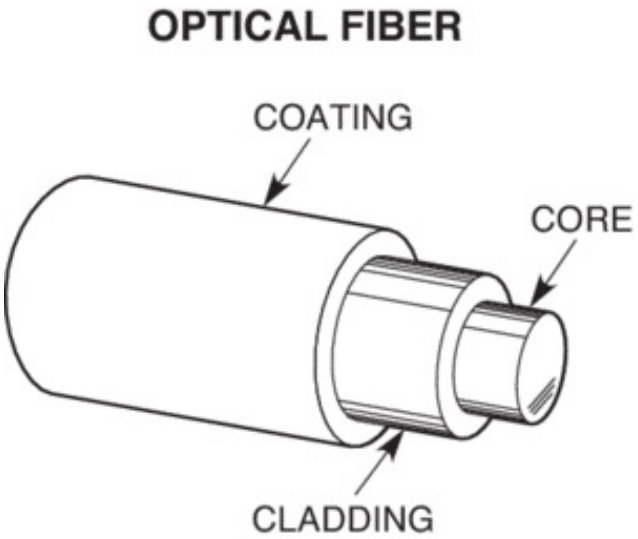

Figure 2. Coated optical fiber scheme.

It is made up of three main components: a core made of glass, a cladding made of glass with a refraction index a bit lower than the core's one and an external coating. The coatings most used in the aeronautical field are Polyimide and Ormocer. They are characterized by excellent adhesion between the fiber and the coating; in fact, the latter must be able to transfer the load to the fiber core where the sensor is inscribed.

When an optical fiber is simultaneously exposed to temperature, mechanical strain/stress and humid environment, the coating of the optical fiber will contribute to the total normalized

wavelength's shift. By applying the superposition of the effects on Equations (5) and (7), we get the governing equation:

$$\frac{\Delta\lambda}{\lambda_B} = \varepsilon_{tot} + \xi\Delta T - p_e(\varepsilon_{res} + \varepsilon_m) \tag{9}$$

where

- ε_{tot} is the actual strain affecting the glass core, which takes into account, according to the law of mixtures, the different contributions due to the different materials. It takes into account the total strain given by thermal, hygroscopic and mechanical contributions.
- $\xi\Delta T$ is the contribution to the normalized wavelength's shift given by the change of n_{eff} due to temperature variation.
- $-p_e(\varepsilon_{res} + \varepsilon_m)$ is the contribution to the normalized wavelength's shift due to the change of n_{res}, which comes from a strain field generated by external or residual stress.
- ε_{res} is the strain related to the residual stress generated according to the mixture laws. In fact, due to the compatibility equations, in a system composed of different materials, all of them will experiment the same strain, this will generate a different stress field in each material and—consequently some residual stress. This is always verified if the system can be modeled as springs in parallel and if it is reasonable to assume perfect adhesion between the parts. On the contrary, for an uncoated optical fiber, since it is made by a single material, $\varepsilon_{res} = 0$ and no residual stresses originate.
- ε_m is the strain generated by an external force.

The contributions just presented will be quantified in the following Section 2.2.1 using a micromechanical approach, and the final form is presented in Section 2.2.2.

2.2.1. Micromechanics Approach

Let us consider a coated optical fiber (Figure 2) simultaneously subjected to mechanical and hygrothermal loads. The following quantities are defined, where subscript "g" refers to glass (i.e., core and cladding) and subscript "c" refers to the coating:

- $E_g, A_g, V_g = \frac{A_g}{A_{tot}}$ are, respectively, the Young modulus, the section area and the volumetric fraction of the glass.
- $E_c, A_c, V_c = \frac{A_c}{A_{tot}}$ are, respectively, the Young modulus, the section area and the volumetric fraction of the coating.
- α_g, α_c are, respectively, the coefficient of thermal expansion (CTE) of the glass and coating.
- β_c is the swelling coefficient of the coating such as $\varepsilon_{RH} = \beta_c\Delta RH$.
- $A_{tot} = A_c + A_g, E_{tot}$, respectively, are the total area and the equivalent Young modulus of the system composed of the optical fiber and coating.

The total force experienced by the system is the addition of the hygrothermal and mechanical forces is as follows:

$$F_{tot} = A_g E_g \alpha_g \Delta T + A_c E_c \alpha_c \Delta T + A_c E_c \beta_c \Delta RH + F_{ext} \tag{10}$$

F_{ext} is an external axial force applied along the fiber axis. According to mixture law equations, it results in

$$\begin{cases} \varepsilon_{tot} = \varepsilon_c = \varepsilon_g \\ F_{tot} = F_g + F_c \end{cases} \tag{11}$$

where F_c and F_g, respectively, are the portion of load borne by the coating and by the glass (core and cladding). Manipulating the above equations, we obtain

$$\begin{cases} \varepsilon_{tot} = \varepsilon_c = \varepsilon_g \\ \frac{F_{tot}}{A_{tot}} = \frac{F_g}{A_{tot}}\frac{A_g}{A_g} + \frac{F_c}{A_tot}\frac{A_c}{A_c} \rightarrow \sigma_{tot} = V_c\sigma_c + V_g\sigma_g \end{cases} \tag{12}$$

Solving the system (12) is possible to obtain the equivalent Young modulus:

$$E_{tot}\varepsilon_{tot} = V_c E_c \varepsilon_c + V_g E_g \varepsilon_g \rightarrow E_{tot} = V_c E_c + V_g E_g \tag{13}$$

This is the Young modulus of the whole system, composed of an optical fiber core and cladding made of glass and coating. It is now possible to compute the actual strain assumed by the system with the linear elastic constitutive law, as follows:

$$\varepsilon_{tot} = \frac{F_{tot}}{A_{tot}E_{tot}} = \frac{A_g E_g \alpha_g \Delta T + A_c E_c \alpha_c \Delta T + A_c E_c \beta_c \Delta RH + F_{ext}}{A_c E_c + A_g E_g} \tag{14}$$

Let us now quantify ε_{res}. It is the fictitious strain applied on the glass fiber core due to the residual stress. In other words, it is the strain that the core would assume after reducing the strain that the core actually assumes. In mathematical terms, it is

$$\varepsilon_{res} = \alpha_g \Delta T + \cancel{\varepsilon_m} - \left(\frac{A_c E_c \beta_c}{A_c E_c + A_g E_g} \Delta RH + \frac{A_c E_c \alpha_c + A_g E_g \alpha_g}{A_c E_c + A_g E_g} \Delta T + \cancel{\varepsilon_m} \right) \tag{15}$$

Equation (15) shows that, whenever the system composed of fiber glass and coating is subjected to a hygrothermal load, a residual stress is generated. This residual stress $\sigma_{res} = E_g \varepsilon_{res}$ is calculated as the product of the elastic modulus of the glass (E_g) and the residual strain (ε_{res}). Such stress will induce a change in the refractive index, quantified through the photo-elastic coefficient (p_e).

2.2.2. Modified Bragg Equation

Now we derive the modified Bragg equation for a coated optical fiber subjected to mechanical and hygrothermal loads, introducing Equations (14) and (15) into Equation (9):

$$\begin{aligned} \frac{\Delta\lambda}{\lambda_b} = & \frac{A_g E_g \alpha_g \Delta T + A_c E_c \alpha_c \Delta T + A_c E_c \beta_c \Delta RH + Fext}{A_c E_c + A_g E_g} + \xi \Delta T \\ & - p_e \left[\alpha_g \Delta T - \left(\frac{A_c E_c \beta}{A_c E_c + A_g E_g} \Delta RH + \frac{A_c E_c \alpha_c + A_g E_g \alpha_g}{A_c E_c + A_g E_g} \Delta T \right) + \varepsilon_m \right] \end{aligned} \tag{16}$$

It is important to note that, due to the compatibility equation, $\varepsilon_m^c = \varepsilon_m^g = \varepsilon_m = \frac{F_{tot}}{A_{tot}E_{tot}}$. By manipulating Equation (16) to facilitate the external mechanical and hygrothermal loads, we get

$$\begin{aligned} \frac{\Delta\lambda}{\lambda_b} = & \\ & \left[(1+p_e) \frac{A_c E_c \alpha_c + A_g E_g \alpha_g}{A_c E_c + A_g E_g} - p_e \alpha_g + \xi \right] \Delta T + \\ & \left[(1+p_e) \frac{A_c E_c \beta_c}{A_c E_c + A_g E_g} \right] \Delta RH + \\ & (1-p_e)\, \varepsilon_m \end{aligned} \tag{17}$$

This new formulation permits us to derive some linear coefficients that are able to link hygrothermal and mechanical loads to the normalized Bragg wavelength shift by knowing the properties of constituent materials. For the sake of brevity, Equation (17) can be rewritten as follows:

$$\frac{\Delta\lambda}{\lambda_b} = K_T^{coated} \Delta T + K_{RH}^{coated} \Delta RH + K_m^{coated} \varepsilon_m \tag{18}$$

where K_T^{coated}, K_{RH}^{coated} and K_m^{coated}, respectively, represent the sensitivity to temperature, relative humidity and mechanical strain of a coated optical fiber.

2.3. Analytical Validation

Equation (17) is the modified Bragg equation for a coated optical fiber subjected to hygrothermal and mechanical loads. An analytical validation of the modified Bragg equation is the derivation of the governing equation of an uncoated optical fiber by simplify some terms.

Proof. Let us consider that is is possible to write the following relationship with the coating made of the same material of the core and cladding (i.e., glass):

$$\begin{cases} \alpha_c = \alpha_g \\ E_c = E_g \\ \beta_c = \beta_g = 0 \end{cases} \tag{19}$$

By introducing the system in Equation (19) into Equation (17), we get

$$\begin{aligned} \frac{\Delta\lambda}{\lambda_b} = & \left[(1+p_e) \frac{A_{tot}E_g\alpha_g}{A_{tot}E_g}^{1} - p_e\alpha_g + \xi \right] \Delta T \\ & + \left[(1+p_e) \frac{A_cE_c\beta_c + A_rE_r\beta_r}{A_gE_g + A_cE_c + A_rE_r}^{0} \right] \Delta RH \\ & + (1-p_e)\,\varepsilon_m \end{aligned} \tag{20}$$

Resolving the equation, we get

$$\frac{\Delta\lambda}{\lambda_B} = (\xi + \alpha_g)\Delta T + (1-p_e)\varepsilon_m \tag{21}$$

Equation (21) is the governing equation for an uncoated optical fiber commonly reported in the literature, such as [21–23]. □

3. Experimental Activities

In order to validate the modified Bragg equation presented in Section 2.2.2, some experimental activities are carried out. The aim is to identify sensitivities to temperature, relative humidity and mechanical strain of FBG sensors inscribed inside an optical fiber. To do this, fibers are arranged within the climate chamber, exposing the sensor to different hygrothermal conditions. By measuring the Bragg wavelength in real time, it is possible to obtain characteristic charts. Two different fibers are employed, a polyimide-coated fiber and an uncoated fiber, which was obtained from a coated one simply by removing the coating in the sensing region. The first is expected to be sensitive to RH changes, being covered with hydrophilic materials. The uncoated one should present no RH sensitivity because both core and cladding (made of silica) are hydrophobic. Finally, each fiber is sensitive to temperature changes. The properties of the optical fiber are listed in Table 1. Values are derived from the data sheet of the optical fiber used, standard experiments or literature values [23–28].

The main experimental equipment needed to work out these tests comprised the climate chamber ACS DY110C, with environmental conditions being recreated and the interrogator Micron Optics sm130, allowing for the measurement of instant Bragg's wavelength. Both are shown in Figure 3.

Table 1. System's parameters: subscript "g" is refers to the glass and subscript "c" to the coating.

Parameter	Symbol	Value
Core + cladding radius	r_g	62.5 µm
Coating radius	r_c	77.5 µm
Glass Young modulus	E_g	70 GPa
Coating Young modulus	E_c	2.5 GPa
Photo-elastic coefficient	p_e	0.2126 [-]
Thermo-optic coefficient	ξ	5.81×10^{-6} 1/K
Glass CTE	α_g	1.020×10^{-6} 1/K
Coating CTE	α_c	3.636×10^{-5} 1/K
Coating swelling coefficient	β_c	5.589×10^{-5} 1/RH%

(**a**) Climate chamber. (**b**) Optical fiber interrogator.

Figure 3. Experimental setup.

Both fibers are tested in a climatic chamber, subjecting the optical fiber to various thermo-humidity conditions. A temperature sweep is performed from 25 °C to 90 °C in 5 °C increments. For each temperature, the relative humidity is varied from 20% to 90% in 10% increments. Once temperature and relative humidity are stabilized, the fiber is exposed to these conditions for 2 h. In Sections 3.1 and 3.2, the test results of uncoated and coated optical fibers are presented, respectively.

3.1. Uncoated Optical Fiber

This section aims to determine the sensitivity to temperature of FBG inscribed inside an uncoated optical fiber and to prove the insensitivity of glass to relative humidity. Figure 4 reports the FBG response to the hygrothermal cycle presented in Section 3.

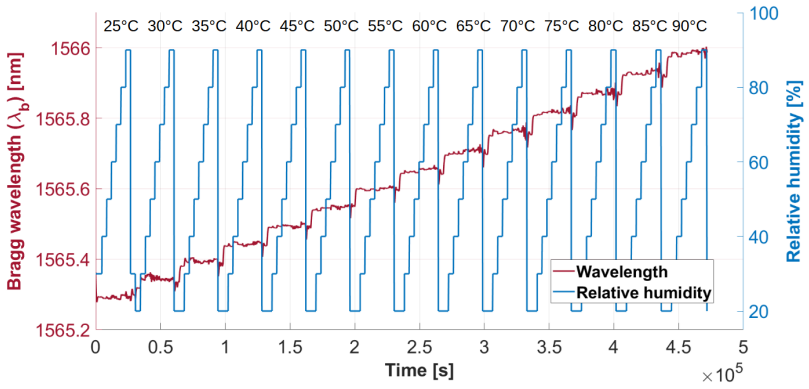

Figure 4. Wavelength trend in time for an uncoated fiber.

The curve reported in Figure 4 shows the insensitivity to RH of the uncoated fiber. In particular, it is possible to note that the Bragg wavelength increases as the temperature increases, but it remains more or less constant inside each segment at a constant temperature,

even though relative humidity changes. The oscillations of (λ) inside each segment are due to the fact that temperature does not remain perfectly constant. As a matter of fact, to modify relative humidity, the climate chamber injects hot vapor into the chamber to increase relative humidity or dry cold air to decrease it. During this process, the temperature inevitably changes. This behavior proves the inability of glass to sense relative humidity, due to its hydrophobic characteristics. As a consequence, it is possible to state that $\beta_g = 0$.

The signal shown in Figure 4 allows us to compute a normalized Bragg wavelength shift by subtracting and dividing it by $\lambda_B = \lambda_{00}$, which is the value of λ given by the FBG sensor at 0% RH and at 0 °C. Consequently,

$$\frac{\Delta\lambda}{\lambda_{00}} = \frac{\lambda - \lambda_{00}}{\lambda_{00}} \tag{22}$$

where $\lambda_{00} = 1565.0159990$ nm. This is not a measured value due to the fact that it is impossible to reach 0 °C and 0% relative humidity in a climatic chamber. The value was derived from thermal and humidity sensitivities by computing the y-intercept. Once the value of the normalized Bragg's wavelength shift was calculated, the average of the acquired data points was determined for the time interval, during which humidity and temperature conditions remained constant. This approach allowed for obtaining a normalized Bragg's wavelength shift for each pair of humidity and temperature values.

Figure 5a shows normalized Bragg's wavelength shift versus temperature at constant relative humidity, while Figure 5b shows normalized Bragg's wavelength shift versus relative humidity at constant temperature.

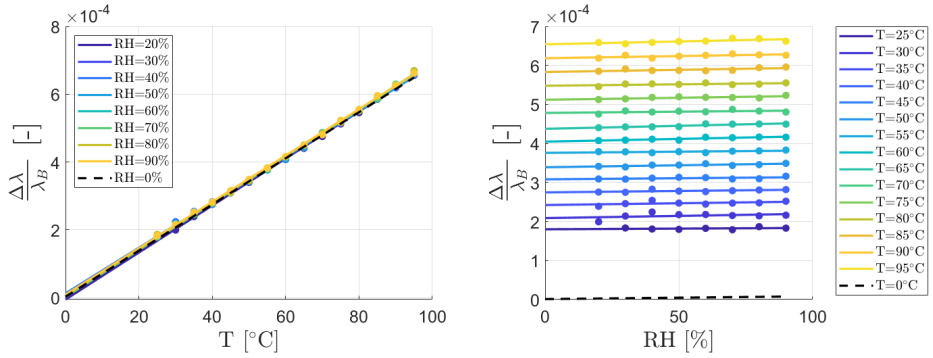

(**a**) Temperature sensitivities. (**b**) Humidity sensitivities.

Figure 5. Linear interpolation and sensitivities, uncoated fiber.

Figure 5b shows that the slope of the linear curve, which represents the sensitivity to relative humidity (RH), is nearly horizontal, indicating a negligible sensitivity. Mathematically, the sensitivity to relative humidity for the uncoated fiber is

$$K_{RH}^{uncoated} = 9.502 \cdot 10^{-8} \left[\frac{1}{RH}\right]$$

The small value of the sensitivity confirms that the uncoated fiber exhibits almost no response to variations in relative humidity. In fact, a change of 100% RH will generate a shift of 15 pm. To provide a reference point, let us consider that a shift of 15 pm is caused by a mechanical deformation equal to 12.5$\mu\varepsilon$.

Alternatively, the analysis of Figure 5a allow us to appreciate the linear relationship between temperature and the normalized Bragg wavelength shift at each relative humidity level of an uncoated optical fiber. As a matter of fact, by holding relative humidity constant and only varying temperature, it is possible to compute the slope of each curve that is the temperature sensitivity of the bare fiber at constant relative humidity ($K_T^{uncoated}$). The results are summarized in Table 2.

Table 2. Sensitivities to temperature at each relative humidity value for the uncoated fiber.

RH [%]	$K_T^{uncoated}$ [1/°C]	RH [%]	$K_T^{uncoated}$ [1/°C]
20	6.873×10^{-6}	60	6.846×10^{-6}
30	6.844×10^{-6}	70	6.874×10^{-6}
40	6.724×10^{-6}	80	6.858×10^{-6}
50	6.828×10^{-6}	90	6.840×10^{-6}

The results shown in Figure 5a and in Table 2 allow us to state that the sensitivity to temperature is not affected by humidity changes. In other words, it is possible to consider a unique value of $K_T^{uncoated}$ for different values of RH without making significant errors. This is also supported by computing the standard deviation of $K_T^{uncoated}$ and coefficient of variation (CoV) that gives low values, as follows:

$$\begin{cases} \mu = K_T^{uncoated} = 6.8298 \cdot 10^{-6} \frac{1}{°C} \\ \sigma = 0.04794 \cdot 10^{-6} \\ CoV = \frac{\sigma}{|\mu|} = 0.007 \rightarrow 0.7\% \end{cases}$$

3.2. Coated Optical Fiber

A polyimide-coated optical fiber was used to perform the experimental activities. The test procedures presented in Section 3 were conducted three times to confirm their repeatability, as shown in Figure 6a.

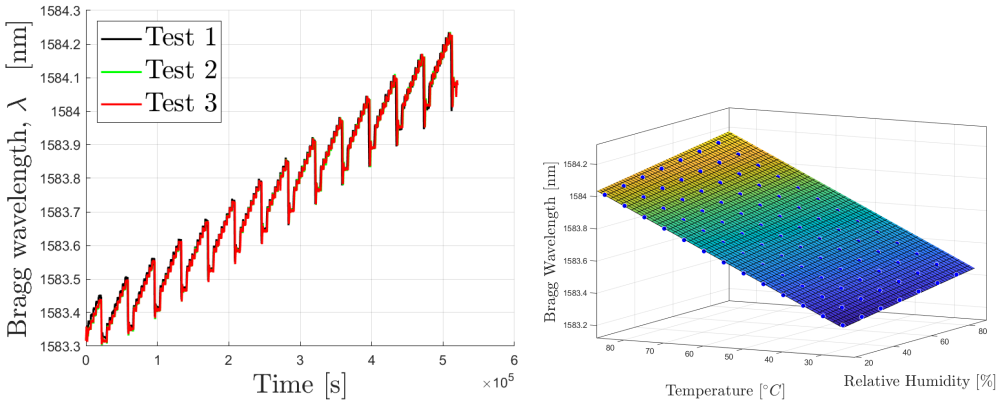

(**a**) Overlapping of the three tests. (**b**) Interpolating plane.

Figure 6. Coated fiber response.

The interpolating plane represented in Figure 6b shows the response of the FBG sensor when it is exposed to different levels of temperature and relative humidity. This plane was computed by averaging the responses of the sensors during the three experiments for each pair of T and RH (Figure 6a). It appears evident that the trend of the Bragg wavelength with respect to both temperature and relative humidity is almost linear, although there is weak, negligible non-linear behavior given by the dependency of the absorption capacity of the coating on the temperature. The linearity is valid when also considering the dimensionless form of λ, leading to a validation of the linear trend proposed by the hygrothermal law presented in Equation (17):

$$\frac{\Delta\lambda}{\lambda_{00}} = K_T^{coated}\Delta T + K_{RH}^{coated}\Delta RH + K_m^{coated}\cancelto{0}{\varepsilon_m} \tag{23}$$

where K_T^{coated}, K_{RH}^{coated} and K_m^{coated}, respectively, represent the sensitivity to temperature, relative humidity and mechanical strain of a coated optical fiber. The dimensionless form of λ is computed as follows:

$$\frac{\Delta\lambda}{\lambda_{00}} = \frac{\lambda - \lambda_{00}}{\lambda_{00}} \tag{24}$$

where $\lambda_B = \lambda_{00}$ is the Bragg wavelength at 0 °C and 0% RH, which is the planar intercept at the origin:

$$\lambda_{00} = 1582.95895\,\text{nm} \tag{25}$$

Once λ_{00} is determined, a normalized Bragg wavelength shift can be computed solving Equation (24) and sensitivities to temperature and relative humidity variation can be evaluated.

In Figure 7a, the variation of a normalized Bragg shift due to temperature changes at constant relative humidity is presented. The slope of the curves is the sensitivity to temperature of a coated optical fiber. Since the curves are straight lines parallel to each other, this allows us to conclude that the sensitivity to temperature does not depend on relative humidity; therefore, a single value can be considered for sensitivity. This is also supported by low values of standard deviations and coefficient of variance (CoV) shown in Equation (26):

$$\begin{cases} K_T^{coated} = 7.637 \cdot 10^{-6}\ 1/°\text{C} \\ \sigma = 7.691 \cdot 10^{-8}\ 1/°\text{C} \\ CoV = \frac{\sigma}{|\mu|} = 0.010 \rightarrow 1.0\% \end{cases} \tag{26}$$

These values are obtained from the slopes of the curves obtained in all three experiments carried out. In the same way, in Figure 7b, the variation of a normalized Bragg shift due to relative humidity changes at a constant temperature is presented. The slope of the curves is the sensitivity to relative humidity of a coated optical fiber. Due to the non-linearity given by the dependency of the absorption capacity on the temperature, we have a slight higher CoV that leads to an error less then 5%, as shown in Equation (27).

$$\begin{cases} K_{RH}^{coated} = 1.276 \cdot 10^{-6}\,1/\text{RH} \\ \sigma = 6.083 \cdot 10^{-8}\ 1/\text{RH} \\ CoV = \frac{\sigma}{|\mu|} = 0.0476 \rightarrow 4.8\% \end{cases} \tag{27}$$

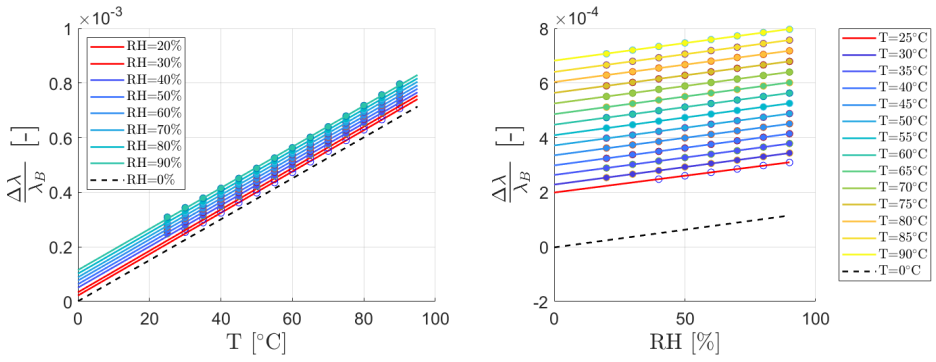

(**a**) (**b**)

Figure 7. Linear interpolation and sensitivities. (**a**) Linear interpolation for temperature sensitivities. (**b**) Linear interpolation for humidity sensitivities.

4. Results and Discussion

A comparison between Bragg wavelength measured from the uncoated FBG sensor (Section 3.1 and Bragg wavelength estimated by Equation (21) is presented in Figure 8. The experimental wavelength is evaluated by averaging the values shown in Figure 4 at each

constant temperature. The analytical wavelength is computed by setting the thermo-optic coefficient $\xi = 5.81 \times 10^{-6}\,1/\mathrm{K}$ and the glass cte $\alpha_g = 1.020 \times 10^{-6}\,1/\mathrm{K}$, as shown in Table 1 and in accordance with literature values [23–26].

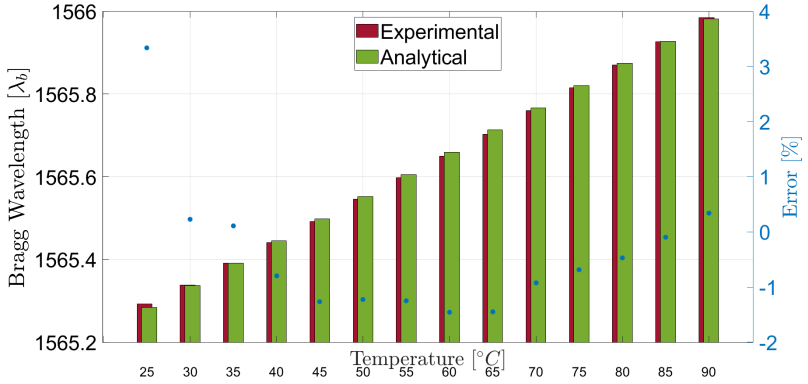

Figure 8. Comparison between theoretical and experimental wavelengths at each constant temperature.

The comparison reveals good agreement between the experimental and analytical results, confirming the validity of the modified Bragg wavelength for uncoated optical fibers Equation (21). This is also confirmed by the values of error reported in Figure 8, computed comparing the normalized Bragg wavelength measured by the sensor and the one estimated by the analytical model, as follows:

$$err_{\%} = \frac{\frac{\Delta\lambda_{measured}}{\lambda_{00}} - \frac{\Delta\lambda_{estimated}}{\lambda_{00}}}{\frac{\Delta\lambda_{estimated}}{\lambda_{00}}} \times 100 \tag{28}$$

Normalized Bragg wavelength is used in place of reflected Bragg wavelength thanks to its capability to represent sensitiveness. Using the normal wavelength would have led to extremely small (given the large denominator value) and unrepresentative errors. The maximum error is 3.34% and was found at 25 °C.

It is now possible to compare the Bragg wavelength computed with the use of the modified Bragg equation presented in Equation (17) and the Bragg wavelength measured by experimental tests and reported in Section 3.2. Figure 9 presents this comparison, where each curve represents a constant temperature indicated by the caption, and each segment of each curve represents a constant value of relative humidity.

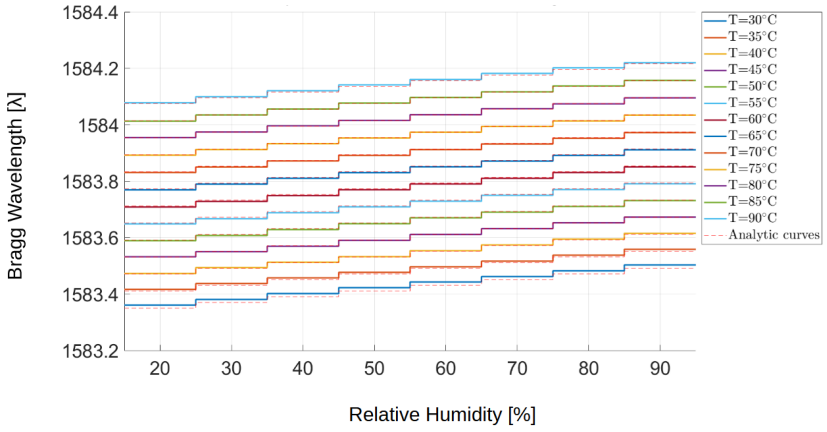

Figure 9. Comparison between theoretical and experimental wavelengths at each constant temperature and relative humidity.

The comparison shows the ability of the analytical model to reproduce the experimental physical behavior of the coated optical fiber. As in Equation (28), the error between the normalized Bragg wavelength measured by the sensor and the estimated one computed by using the analytical model are listed in Table 3.

Table 3. Error between normalized Bragg wavelength estimated and measured by the sensor at each temperature and relative humidity.

T/ RH	20%	30%	40%	50%	60%	70%	80%	90%
30 °C	2.59%	2.42%	2.46%	2.52%	2.40%	2.10%	2.03%	2.10%
35 °C	1.22%	1.29%	1.19%	1.03%	0.90%	0.86%	0.98%	1.06%
40 °C	0.28%	0.46%	0.15%	0.10%	0.24%	0.31%	0.39%	0.41%
45 °C	0.09%	−0.22%	−0.39%	−0.25%	−0.16%	−0.09%	−0.05%	−0.05%
50 °C	−0.41%	−0.73%	−0.59%	−0.48%	−0.36%	−0.35%	−0.36%	−0.25%
55 °C	−0.56%	−0.78%	−0.65%	−0.54%	−0.54%	−0.45%	−0.40%	−0.33%
60 °C	−0.59%	−0.62%	−0.57%	−0.47%	−0.45%	−0.45%	−0.38%	−0.42%
65 °C	−0.51%	−0.47%	−0.41%	−0.41%	−0.36%	−0.32%	−0.31%	−0.37%
70 °C	−0.32%	−0.43%	−0.23%	−0.31%	−0.27%	−0.29%	−0.28%	−0.30%
75 °C	−0.20%	−0.21%	−0.15%	−0.15%	−0.13%	−0.11%	−0.16%	−0.14%
80 °C	−0.02%	−0.06%	0.09%	−0.01%	−0.00%	0.11%	−0.14%	−0.08%
85 °C	−0.19%	−0.06%	0.00%	0.08%	0.04%	0.03%	0.09%	0.02%
90 °C	0.23%	0.33%	0.39%	0.41%	0.35%	0.42%	0.39%	0.23%

The maximum error of 2.59% is found at 30 °C and 20% relative humidity. The largest errors are located in low-temperature and low-humidity regions as the previous case. As a matter of fact, this is the region where the climate chamber controller hardly maintains hygrothermal conditions, in accordance with the Moiller diagram. However, the error magnitude is within an acceptable range for practical applications, demonstrating the robustness of the model for HUMS deployment in aerospace structures.

The polyimide-coated fibers exhibited significant sensitivity to humidity due to moisture absorption by the coating material. This behavior introduces an additional swelling-induced strain component, which is accurately captured by the modified Bragg Equation (17). These results confirm the importance of accounting for both temperature and humidity effects when monitoring composite materials embedded with FBG sensors.

This study highlights that strain measurements obtained from FBG sensors inscribed in coated optical fibers are influenced by humidity. To achieve accurate strain measurements reflecting the actual deformation state of the monitored component, it is essential to compensate for the strain contribution induced by the fiber coating. However, this compensation can be considered negligible in short-term monitoring scenarios, where it is reasonable to assume minimal variation in moisture concentration within the composite material over the measurement period. In contrast, the situation differs significantly for long-term monitoring scenarios, particularly in aerospace applications, where the monitoring period may span the entire operational life of a component—up to 30 years. In such cases, neglecting the effects of long-term moisture absorption could result in substantial measurement inaccuracies, compromising the reliability of the monitoring system.

5. Conclusions

The derived equations include terms for strains induced by thermal and humidity loads, external mechanical forces and residual stresses. The model is valid within the limits of the Mollier diagram and under the assumptions of orthotropic continuum mechanics: small displacements, linear elastic law and validity of the compatibility equation (i.e., perfect fiber/coating adhesion). The superposition of effects, the net of non-linearities arising from the dependence of adsorption/hydration capacity on temperature, is a direct consequence of the derivation of modified Bragg's law (Equation (17)).

Polymeric coated fibers are nowadays widely used in SHM systems; they are either glued to the surface of the components or embedded in them. This paper showed that such

sensors are inevitably subject to moisture absorption, which changes the sensor's response. As the kinetic of moisture absorption is very slow, the effect of moisture is negligible if the wavelengths are normalized with respect to a measured value at a time instant not far from the one of the desired measurements. In contrast, in the case of monitoring a component for its entire service life (i.e., from the cradle to the grave), in order to have a reliable measurement, it is necessary to take into account the moisture absorbed through the equations just presented.

Overall, the results provide a framework for expanding the applicability of the modified Bragg model to broader monitoring systems. By quantifying sensitivity coefficients for both temperature and humidity, this study enables the precise calibration of HUMS systems for reliable operation in diverse environmental conditions. These insights pave the way for improved material selection and protective strategies in composite applications, ensuring durability and safety.

One limitation of the current approach is the inability to decouple the strain components measured by the sensor that are induced by temperature from those caused by humidity. Future research efforts should focus on developing methods to separate these effects, enabling the measurement system to provide detailed information about the amount of moisture absorbed by the composite material. Such advancements would enhance the accuracy and utility of FBG-based monitoring systems in predicting the long-term performance and durability of aerospace components.

6. Patents

The present work was submitted for filing at the patent office with application number 102024000013114 and is currently under review by the relevant office.

Author Contributions: Conceptualization, P.A.; methodology, P.A.; software, P.A.; validation, P.A.; formal analysis, P.A.; investigation, P.A.; resources, P.A.; data curation, P.A.; writing—original draft preparation, P.A.; writing—review and editing, P.A. and G.S.; visualization, P.A.; supervision, G.S. All authors have read and agreed to the published version of the manuscript.

Funding: This research received no external funding.

Data Availability Statement: Data is contained within the article.

Conflicts of Interest: The authors declare no conflicts of interest.

Abbreviations

The following abbreviations are used in this manuscript:

CoV	Coefficient of variance
CTE	Coefficient of thermal expansion
FBG	Fiber Bragg Sensor
FO	Fiber optics
HUMS	Health and Usage Monitoring System
SHM	Structural Health Monitoring

References

1. Aceti, P.; Ballarin, P.; Ghiasvand, S.; Airoldi, A.; Bettini, P.; Sala, G. Effect of Hygrothermal Ageing on Optical Fibersensorized Composite Materials. In Proceedings of the 26th Conference of the Italian Association of Aeronautics and Astronautics (AIDAA 2021), Online, 31 August–3 September 2021; pp. 1–6.
2. Krauklis, A. Environmental Aging of Constituent Materials in Fiber-Reinforced Polymer Composites. Ph.D. Thesis, Norwegian University of Science and Technology, Trondheim, Norway, 2019.
3. Zimmermann, N.; Wang, P.H. A review of failure modes and fracture analysis of aircraft composite materials. *Eng. Fail. Anal.* **2020**, *115*, 104692. [CrossRef]
4. Niu, Y.F.; Yan, Y.; Yao, J.W. Hygrothermal aging mechanism of carbon fiber/epoxy resin composites based on quantitative characterization of interface structure. *Polym. Test.* **2021**, *94*, 107019. [CrossRef]
5. Aceti, P.; Carminati, L.; Bettini, P.; Sala, G. Hygrothermal ageing of composite structures. Part 1: Technical review. *Compos. Struct.* **2023**, *319*, 117076. [CrossRef]

6. Riva, M.; Airoldi, A.; Turconi, T.; Ballarin, P.; Boiocchi, M.; Bottasso, L. Development and manufacturing of flexible joints based on corrugated composite laminates. *Compos. Struct.* **2023**, *308*, 116683. [CrossRef]
7. Airoldi, A.; Boiocchi, M.; Natali, M.; Mirani, C.; Di Pancrazio, L.; Consiglio, G.; Ballarin, P.; Riva, M. Feasibility of a morphing rocket nozzle for thrust vector control based on corrugated composite laminates. *Appl. Compos. Mater.* **2023**, *30*, 399–429. [CrossRef]
8. Ray, B.C.; Prusty, R.K.; Rathore, D.K. *Fibrous Polymeric Composites: Environmental Degradation and Damage*; CRC Press: Boca Raton, FL, USA, 2018.
9. Shetty, K.; Bojja, R.; Srihari, S. Effect of hygrothermal aging on the mechanical properties of IMA/M21E aircraft-grade CFRP composite. *Adv. Compos. Lett.* **2020**, *29*, 2633366X20926520. [CrossRef]
10. Kececi, E.; Asmatulu, R. Effects of moisture ingressions on mechanical properties of honeycomb-structured fiber composites for aerospace applications. *Int. J. Adv. Manuf. Technol.* **2017**, *88*, 459–470. [CrossRef]
11. Aceti, P.; Bianchi, C.; Sala, G. Hygrothermal Effects in Aeronautical Composite Materials Subjected to Freeze–Thaw Cycling. *Aerotec. Missili Spaz.* **2023**, *103*, 255–267. [CrossRef]
12. Australian Transport Safety Bureau. *How Old is Too Old? The Impact of Ageing Aircraft on Aviation Safety*; Australian Transport Safety Bureau: Canberra, Australia, 2007.
13. Li, C.; Ueno, R.; Lefebvre, V. *Investigation of an Accelerated Moisture Removal Approach of a Composite Aircraft Control Surface*; Society for the Advancement of Material and Process Engineering: Diamond Bar, CA, USA, 2006.
14. Ischdonat, N. The Influence of Water Ingress to Aircraft Cabin Components. *Int. J. Aerosp. Mech. Eng.* **2012**, *6*, 1252–1258.
15. Aceti, P.; Carminati, L.; Bettini, P.; Sala, G. Hygrothermal ageing of composite structures. Part 2: Mitigation techniques, detection, removal. *Compos. Struct.* **2023**, *319*, 117105. [CrossRef]
16. Ballarin, P.; Sala, G.; Macchi, M.; Roda, I.; Baldi, A.; Airoldi, A. Application of Artificial Neural Networks to a Model of a Helicopter Rotor Blade for Damage Identification in Realistic Load Conditions. *Sensors* **2024**, *24*, 5411. [CrossRef] [PubMed]
17. Giaccari, P.; Limberger, H.G.; Kronenberg, P. *Influence of Humidity and Temperature on Polyimide-Coated Fiber BRAGG Gratings*; Optica Publishing Group: Washington, DC, USA, 2002.
18. Guan, Y.; Zhang, T.; Dong, X.; Sun, T.; Grattan, K.T.V. Sensor for simultaneous measurement of temperature and humidity based on a chirped fiber Bragg grating partially bonded with thick polyimide film. *IEEE Sens. J.* **2023**, *23*, 24583–24590. https://doi.org/10.1109/JSEN.2023.3312067 [CrossRef]
19. Yeo, T.L.; Sun, T.; Grattan, K.T.V.; Parry, D.; Lade, R.; Powell, B.D. Polymer-coated fiber Bragg grating for relative humidity sensing. *IEEE Sens. J.* **2005**, *5*, 1082–1089. [CrossRef]
20. Hill, K.O.; Meltz, G. Fiber Bragg Grating Technology Fundamentals and Overview. *J. Light. Technol.* **1997**, *15*, 1263. [CrossRef]
21. Rajan, G. *Optical Fiber Sensors: Advanced Techniques and Applications*; CRC Press: Boca Raton, FL, USA, 2017.
22. McCall, M. On the application of coupled mode theory for modeling fiber Bragg gratings. *J. Light. Technol.* **2000**, *18*, 236–242. [CrossRef]
23. Morey, W.W.; Meltz, G.; Glenn, W.H. Fiber Optic Bragg Grating Sensors. In Proceedings of the Fiber Optic and Laser Sensors VII, Boston, MA USA, 5–7 September 1989; International Society for Optics and Photonics; DePaula, R.P., Udd, E., Eds.; SPIE: St Bellingham, WA, USA, 1990; Volume 1169, pp. 98–107. [CrossRef]
24. Sahota, J.K.; Gupta, N.; Dhawan, D. Fiber Bragg grating sensors for monitoring of physical parameters: A comprehensive review. *Opt. Eng.* **2020**, *59*, 060901. [CrossRef]
25. Kersey, A.; Davis, M.; Patrick, H.; LeBlanc, M.; Koo, K.; Askins, C.; Putnam, M.; Friebele, E. Fiber grating sensors. *J. Light. Technol.* **1997**, *15*, 1442–1463. [CrossRef]
26. Kronenberg, P.; Rastogi, P.K.; Giaccari, P.; Limberger, H.G. Relative humidity sensor with optical fiber Bragg gratings. *Opt. Lett.* **2002**, *27*, 1385. [CrossRef] [PubMed]
27. Thomas, P.J.; Hellevang, J.O. A high response polyimide fiber optic sensor for distributed humidity measurements. *Sens. Actuators B Chem.* **2018**, *270*, 417–423. [CrossRef]
28. Hicyilmaz, A.S.; Bedeloglu, A.C. Applications of polyimide coatings: A review. *SN Appl. Sci.* **2021**, *3*, 363. [CrossRef]